International Journal of Thermofluid Science and Technology (2023)
Volume 10, Issue 1, Paper No. 100103
https://doi.org/10.36963/IJTST.2023100103
Research Article

Thermal radiation effect on Non-Newtonian Casson fluid through a porous material over a magnetic field with buoyancy

Seun Oyinkansola Mate [1], Adebowale Martins Obalalu [2], Olusegun Adebayo Ajala [1], Toyibat Bamidele Bakare [1], Amos Wale Ogunsola [1], Akintayo Oladimeji Akindele [*, 1]

[1] *Department of Pure and Applied Mathematics, Ladoke Akintola University of Technology, Ogbomoso, Oyo State Nigeria.*
[2] *Department of physics, Augustine University, Ilara-epe, Lagos State, Nigeria.*

ATICLE INFO

Received: 07 Dec. 2023;
Received in revised form:
08 Feb. 2023;
Accepted: 18. Feb. 2023;
Published online:
20 Feb. 2023

Keywords:
Casson fluid
Buoyancy effect
Magnetic
Variable viscosity
Chebyshev collocation method

ABSTRACT

The magnetohydrodynamic (MHD) chemically reactive of Casson non-Newtonian nanofluid flow on a two-dimensional incompressible steady from stretched sheet in a porous quiescent medium with buoyancy effect is investigated numerically. Additional effects included in the originality of the model are the applied magnetic field and solar radiation effect. The Chebyshev collocation method (CCM) was used to solve the ordinary differential equations (ODEs) with MATHEMATICA 11.3 software. The present tables and graphs show the performance of fluid physical quantities, momentum flow, energy distribution, nanoparticle concentration, and velocity for various values of applicable dimensionless numbers. The numerical outcomes demonstrate the effect of different physical parameters of the fluid, and it was observed that the velocity profile increased as the thermal and mass Grashof number increased due to an increase in buoyant force caused by heat transferred from the vertical plate to the fluid but decreased as the Casson parameter increased due to a decrease in its yield stress, porosity, and magnetic parameter. Also Analyses reveal that the thermal profile reduce with an increase in variable thermal conductivity parameter. This study will be of considerable economic value to marine engineers, mechanical engineers, physicists, chemical engineers, and others since its application will help them improve their operations.

1. Introduction

Numerous academic researchers have been analyzing non-Newtonian fluids in recent years due to their applications in many areas of human endeavors, including science and technology, food processing and engineering practices, as well as petroleum products and exotic lubricants. However, it is necessary to investigate the flow behavior of non-Newtonian fluids in order to have a comprehensive understanding of these fluids and their different uses. The intensity of

[*] *Corresponding e-mail*: *aoakindele21@lautech.edu.ng* (Akintayo Oladimeji Akindele)

Nomenclature

A	heat source parameter	$q^{'''}$	heat sink/source
A^*	heat sink parameter	Ra_x	local Rayleigh number
B_o	applied magnetic induction	S_h	Shewood number
b^*	empirical constant	T	fluid temperature
C	fluid concentration	T_w	wall temperature
C_p	specific heat at constant pressure	T_∞	free stream temperature
C_w	wall Concentration	U_w	reference velocity
C_∞	Free stream concentration	u, v	fluid velocity in x and y direction
D_B	Brownian motion	ν	kinematic viscosity
$D_B(C)$	variable mass diffusivity	δ	heat generation parameter
$D_{B\infty}$	constant Brownian diffusion coefficient	δ_w	excess wall temperature ratio parameter
D_T	thermophoretic diffusion coefficient	η	similarity variable
E_c	Eckert number	θ	temperature profile
Ea	activation energy	φ	concentration profile
F_s	Forchheimer parameter	τ	Particles heat capacity to fluid heat capacity ratio
f	velocity profile	σ	electrical conductivity of the surface temperature
G_c	mass Grashof number	ε'	constant depending on the electric fluid
G_r	thermal Grashof number	ε	variation of electric conductivity parameter
g	acceleration due to gravity	$\in_2$	variable viscosity parameter
K_p	permeability coefficient	$\in_4$	variable thermal conductivity parameter
K_r	chemical reaction coefficient	$\in_6$	variable mass diffusion parameter
K_∞	constant thermal conductivity for the fluid	ρ_f	fluid density
$K(T)$	variable thermal conductivity	$\mu_B(T)$	variable viscosity
Le	Lewis number	β	Casson Parameter
M	magnetic Parameter	μ_∞	constant viscosity
N	Thermal radiation	ψ	stream function
N_b	Brownian motion	ξ	latent heat of diffusion
N_t	thermophoresis parameter	λ	chemical Reaction
Nu	Nusselt number	λ_T	thermal expansion coefficient
P_p	porosity parameter	λ_C	mass expansion coefficient
P_r	Prandtl number	κ	boltzmann constant
Q_o	dimensional heat generation coefficient	σ^o	electrical conductivity of the fluid
q_r	radiation heat flux		

applied stress and the elastic deformation of non-Newtonian fluids do not have a linear relationship when applied tension is high and elastic deformation is low. When subjected to force, their viscosity can change from liquid to solid. Custard, toothpaste, cornstarch, paint, blood, melted butter, shampoo, mud, clay, polymer solution, magma, lava, honey, saliva, sperm, mucus, paper pulp, cement slurry, and other substances are examples. Fluids behave differently; some flow faster due to their lower viscosity and higher thermal conductivity, some move parallel in a streamline manner without mixing with other fluids along the

same path, some can easily be compressed when subjected to higher pressure, and some do not obey Newton's law of motion; one of these is a Non-Newtonian Casson Fluid. The Power Law model, Bingham plastic model, Hershel Buckley model, and Casson model are compared to determine the best model to describe a non-Newtonian fluid, and it was discovered that the Shear thickening fluid, Shear thinning fluid, Bingham plastic, Rheopectic or anti-thixotropic, provides a better insight in the low shear rate condition but is insufficient when high shear rate is considered Ref. [1]. Despite the fact that the idea of yield stress has been questioned in the model Ref. [2] the Hershel Buckley model produced a correction to the Bingham plastic model when shear rates are low or maximal, the Bingham plastic model does not give appropriate fluid behavior when shear rates are low or maximal. Casson's rheological model provides more information on non-Newtonian fluids at low and high shear rates, with the addition of a correction factor for yield stress and plastic viscosity making it a more accurate model than others. Ref. [3] is a reference. Several academic have studied the influence of buoyancy on fluids, and they have discovered that the stronger the buoyant force in a fluid, the greater the fluid velocity Refs. [4] and [5]. The Impact of buoyancy force and heat radiation on hydrodynamics flow across a stretched porous sheet was studied using the homotopy analysis in Refs. [6]. The Blasius-Rayleigh-Stoke variables with fall effect were used in ref. [7] to investigate the convective flow of nanofluids. Ref. [14] investigated the mathematical study of Casson fluid flow via elastic tube with applications to blood flow, as well as the effects of arterial elasticity and blood's non-Newtonian behavior on medically important flow parameters. It was discovered that when blood yield stress grows, blood velocity and flow rate decrease dramatically, yet frictional resistance to flow increases in the opposite direction [7-25].

The content and amount of chemical components are altered by a chemical reaction see refs. [38] and [39]. Internal structure is only conveyed whenever the chemical link within electrons is broken. One of the most significant determinants of reaction rate is the direction in which the chemical reactions take place. Using chemical processes, heat and mass transfer may be used to carry out key technical tasks including evaporation, thermal dissipation, and moisture distribution in the industrial business. Many mathematical models were developed to take into consideration the effects of chemical processes. The activation energy, defined as the minimum amount of energy required to activate a chemical reaction, was proposed by Arrhenius. As part of transition-state theory, the activation energy is a result of the variation in energy output between atoms and molecules in an activated or transitional form and their original configuration, according to the findings of ref. [17]. Melting effect on Cattaneo–Christov and thermal radiation features for aligned MHD nanofluid flow comprising microorganisms to leading edge was considered by ref. [28]. Finite difference approach was used to analyze the flow model. Ref. [29], consider the analysis of bio-convective MHD Blasius and Sakiadis flow with Cattaneo-Christov heat flux model and chemical reaction. A comparative study of unsteady MHD Falkner–Skan wedge flow for non-Newtonian nanofluids considering thermal radiation and activation energy was examined by ref. [30]. Insight into significance of thermal stratification and radiation on dynamics of micropolar water based TiO_2 nanoparticle via finite element simulation was carried out by ref. [31]. The crucial features of aggregation in TiO2-water nanofluid aligned of chemically comprising microorganisms was studied by ref. [32], using FEM approach. Ref. [33] considered the Finite element analysis on the thermo-convective non-isothermal nanofluid flow in MHD Hall generator system with Soret and Dufour effects. Thermal radiation influences on MHD stagnation point stream over a stretching sheet with slip boundary conditions was considered by ref. [37]**.** The effect chemical reaction and activation energy on forced convective non-Newtonian with temperature and slip boundary condition was studied by ref. [16]. Their results show that Increases in the heat production parameter, Prandtl number, Eckert number, chemical reaction, and radiation-conduction tend to raise the fluid temperature and lower wall shear stress but increases in the

Casson parameter tend to boost it. Some recent studies on nanofluid flows are mentioned in the references [20-25]. Thermal radiation is electromagnetic radiation in the infrared region of the electromagnetic spectrum, although some of it is in the visible region. Thermal radiation is one of the three basic forms of heat transfer (conduction, convection, and radiation), being a basic property of matter depending on its temperature. From a microscopic point of view, thermal radiation is caused by the random motion of particles, which is caused by the temperature of the material. This causes the electrons and protons to speed up or oscillate as dipoles. Thermal radiation is the emission of electromagnetic waves from all matter that has a temperature greater than absolute zero. Thermal radiation reflects the conversion of thermal energy into electromagnetic energy. Thermal energy is the kinetic energy of random movements of atoms and molecules in matter.

The present study seeks to examine the heat and mass transfer of chemical reactions and activation energy on two-dimensional incompressible MHD non-Newtonian Casson nanofluid flow over a stretched sheet embedded in Darcian porous media with buoyancy effect. The now-Newtonian Casson nanofluid flow over a stretched sheet through a porous medium has gotten a lot of interest in the last several decades because of its diverse industrial and biological uses. However, relatively few studies have been conducted on non-Darcian porous media with a two-dimensional incompressible MHD Casson nanofluid flow across a stretched sheet. In this literature, all the scholars that worked on Casson nanofluid flow over a stretched sheet through a porous medium ignored the influence of buoyant force. The ODEs were solved using MATHEMATICA 11.3 software and the CCM.

2. Model Formulations

The equations that control the isotropic as well as incompressible Casson flow are as follows [34]:

$$\tau_{ij} = \begin{cases} 2\left(\mu_B + \frac{P_y}{\sqrt{2\pi}}\right)e_{ij}, & \pi > \pi_c \\ 2\left(\mu_B + \frac{P_y}{\sqrt{2\pi_c}}\right)e_{ij}, & \pi < \pi_c \end{cases}$$

where τ_{ij} , μ_B , P_y , $\pi = e_{ij}e_{ij}$, $e_{ij} = (i, j)th$, π_c are respectively the Stress tensor, dynamic viscosity of the Non-Newtonian fluid, Fluid yield stress of the liquid, product of the rate of strain tensor with tensor, component of the deformation rate, critical value of the product based on the non-Newtonian model. A double dimensional incompressible MHD on Newtonian nanofluid flow over a stretched sheet embedded in Darcian porous medium was investigated (Fig. 1). where *x* signifies the sheet length and y indicates the sheet width, as defined in [15].The fluid's properties remain constant. The symbols T_∞ and C_∞ for fluid temperature and concentration are *t* and *c*, respectively, while the symbols for ambient temperature and nanoparticle volume fraction are T and C, respectively. The sheets surfaces are made to allow slip flow, and the flow's governing equations, including velocity, energy, and mass transfers, are as follows:

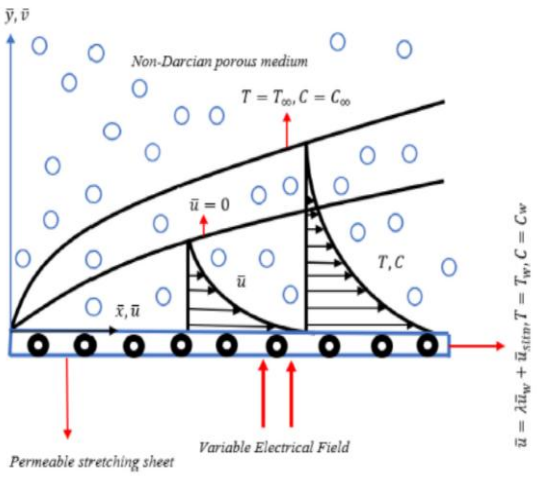

Fig 1: The physical geometry flow.

$$\frac{\partial u}{\partial x} + \frac{\partial v}{\partial y} = 0 \qquad (1)$$

$$u\frac{\partial u}{\partial x}+v\frac{\partial u}{\partial y}=\frac{1}{\rho_f}\frac{\partial}{\partial y}\left[\mu_B(T)\frac{\partial u}{\partial y}\right]\left(1+\frac{1}{\beta}\right)$$
$$-\frac{\sigma^{o}B_o^{\,2}u}{\rho_f}+g\lambda_T(T-T_\infty)+g\lambda_C(C-C_\infty)$$
$$-\frac{\mu_B(T)}{\rho_f(K_P)_o}\left(1+\frac{1}{\beta}\right)u-\frac{b^*}{(K_P)_o}u^2 \qquad (2)$$

$$u\frac{\partial T}{\partial x}+v\frac{\partial T}{\partial y}=\frac{1}{(\rho C_p)_f}\frac{\partial}{\partial y}\left[K(T)\frac{\partial T}{\partial y}\right]+$$
$$\tau\left[D_B\frac{\partial C}{\partial y}\frac{\partial T}{\partial y}+\frac{D_T}{T_\infty}\left(\frac{\partial T}{\partial y}\right)^2\right]+\frac{Q_o}{(\rho C_p)_f}$$
$$(T-T_\infty)+\frac{\sigma^{o}B_o^{\,2}u^2}{(\rho C_p)_f}+\frac{\mu_B(T)}{(\rho C_p)_f}\left(1+\frac{1}{\beta}\right)\left(\frac{\partial u}{\partial y}\right)^2 \qquad (3)$$
$$-\frac{1}{(\rho C_p)_f}\frac{\partial q_r}{\partial y}+\frac{\mu_B(T)}{(\rho C_p)_f}\left(1+\frac{1}{\beta}\right)\frac{u^2}{(K_p)_o}$$
$$+\frac{b^*}{(K_P)_o}u^3+\frac{1}{(\rho C_p)_f}q'''$$

$$u\frac{\partial C}{\partial x}+v\frac{\partial C}{\partial y}=\frac{\partial}{\partial y}\left[D_B(C)\frac{\partial C}{\partial y}\right]$$
$$+\frac{D_T}{T_\infty}\frac{\partial^2 T}{\partial y^2}-K_r(C-C_\infty)\left(\frac{T}{T_\infty}\right)^m\exp^{\frac{-Ea}{\kappa T}} \qquad (4)$$

Subjected to

$$\left.\begin{array}{l} u=u_w(x),\\ v=v_w,\\ T=T_w,\\ C=C_w,\\ \quad at\ \ y=0\\ u\to 0,\ \ T\to T_\infty,\\ \quad C\to C_\infty\quad as\ \ y\to\infty \end{array}\right\} \qquad (5)$$

The stream function is defined as:

$$u=\frac{\partial\psi}{\partial y}\qquad and\qquad v=-\frac{\partial\psi}{\partial x}$$

Now, by Roselland approximate for radiation given by:

$$q_r=-\frac{4\sigma^*}{3\kappa^*}\frac{\partial T^4}{\partial y} \qquad (6)$$

Incorporating the following similarity transformation

$$\eta=y\sqrt{\frac{U_w}{\upsilon}},\psi=\sqrt{\upsilon U_w}xf(\eta), \qquad (7)$$
$$\theta(\eta)=\frac{T-T_\infty}{T_w-T_\infty},\phi(\eta)=\frac{C-C_\infty}{C_w-C_\infty},$$
$$\frac{1}{\sigma^{o}}=\frac{1}{\sigma}\left[1+\varepsilon(T-T_\infty)\right],\varepsilon=\varepsilon(T_w-T_\infty),$$
$$D_B(C)=D_{B\infty}\left[1+\varepsilon_6\left(\frac{T-T_\infty}{T_w-T_\infty}\right)\right],$$
$$q'''=\frac{K_\infty U_w}{\upsilon}\left[A(T_w-T_\infty)f'+A^*(T-T_\infty)\right],$$
$$K(T)=K_\infty(1+\varepsilon_4\theta),\mu_B(T)=\mu_\infty(1+\varepsilon_2-\varepsilon_2\theta),$$
$$E=\frac{Ea}{kT_\infty},\delta_w=\frac{T_w-T_\infty}{T_\infty}.$$

Equation (1) is identically satisfied, substituting (6) and (7) into (2) to (4), we have:

$$\left(1+\frac{1}{\beta}\right)\left[(1+\in_2-\in_2\theta)f'''-\in_2\theta' f''\right]-f'^2$$
$$+ff''-\frac{M}{(1+\varepsilon\theta)}f'+G_r\theta+G_c\varphi-P_p \qquad (8)$$
$$\left(1+\frac{1}{\beta}\right)(1+\in_2-\in_2\theta)f'-F_s f'^2=0$$

$$\theta''+\in_4\theta\theta''+\in_4\theta'^2+P_r f\theta'+P_r N_b\theta'\varphi'$$
$$+P_r N_t\theta'^2+\delta\theta+\frac{P_r ME_c}{(1+\varepsilon\theta)}f'^2+P_r E_c$$
$$\left(1+\frac{1}{\beta}\right)(1+\in_2-\in_2\theta)f''^2+\frac{4}{3}N\theta''+ \qquad (9)$$
$$P_r P_p E_c\left(1+\frac{1}{\beta}\right)(1+\in_2-\in_2\theta)f'^2+$$
$$P_r E_c F_s f'^3+Af'+A^*\theta=0$$

$$\varphi''+\in_6\theta\varphi''+\in_6\theta'\varphi'+Lef\varphi'+\frac{N_t}{N_b}\theta''- \qquad (10)$$
$$Le\lambda(1+\delta_w\theta)^m\exp^{-\frac{E}{(1+\delta_w\theta)}}\varphi=0$$

The derivative with regard to η is denoted by the prime that goes with each profile and the boundary condition (5) becomes:

$$\left\{\begin{array}{l} f(0)=S,\ \ f'(0)=\xi+\left(1+\frac{1}{\beta}\right)\ ,\theta(0)=1,\ \ \phi(0)=1\\ \quad f'(\infty)\to 0,\ \ \theta(\infty)\to 0,\ \ \phi(\infty)\to 0 \end{array}\right. \qquad (11)$$

The evolving physical parameters in (8) – (11) are:

$$P_p = \frac{\mu_\infty}{U_w \rho_f (K_p)_o},\ F_s = \frac{b^* x}{(K_p)_o},\ M = \frac{\sigma B_o^{\ 2}}{\rho_f U_w},$$
$$G_r = \frac{g\lambda_T (T_w - T_\infty)}{U_w^{\ 2} x},\ G_c = \frac{g\lambda_c (C_w - C_\infty)}{U_w^{\ 2} x},$$
$$N_b = \frac{\tau D_B (C_w - C_\infty)}{\nu},\ N_t = \frac{\tau D_T (T_w - T_\infty)}{T_\infty \nu},$$
$$\delta = \frac{\nu Q_o}{U_w K_\infty},\ N = \frac{4\sigma^* T_\infty^{\ 3}}{\kappa^* K_\infty},\ E_c = \frac{U_w^{\ 2} x^2}{(C_p)_f (T_w - T_\infty)},$$
$$P_r = \frac{(\rho C_p)_f \nu}{K_\infty},\ Le = \frac{\nu}{D_B},\ \lambda = \frac{K_r}{U_w},\ \delta_w = \frac{T_w - T_\infty}{T_\infty}$$

These are the Porosity, Forchheimer, Magnetic, Thermal Grashof, Mass Grashof, Brownian motion, Thermophoresis, Heat production, Thermal radiation, Eckert, Prandtl, Lewis, Chemical Reaction, and Excess wall temperature ratio parameters.

3. Nusselt and Shewood numbers

The parameters of significant interest for the present problem are the local Nusselt number Nu and the mass transfer rate S_h which are given by [34]:

$$Nu = -\frac{x}{(T_w - T_\infty)}\left[1 + \frac{16\sigma^*}{3k^* k(T)}\right]\left(\frac{\partial T}{\partial y}\right)_{y=0},$$
$$S_h = \frac{x}{(C_w - C_\infty)}\left(\frac{\partial C}{\partial y}\right)_{y=0} \quad (12)$$

Using the similarity variables of equation (7) into (12), gives:

$$Nu\,\mathrm{Re}_x^{-1/4} = -\left[1 + \frac{4}{3N(1+\varepsilon\theta)}\left(1 + (T_r - 1)\theta(0)^3\right)\right]\theta'(0) \quad (13)$$

$$S_h\,\mathrm{Re}_x^{-1/4} = -\phi'(0) \quad (14)$$

Where

$$\mathrm{Re}_x^{-1/4} = \frac{(1 - C_\infty) g\beta_0 (T_w - T_\infty) x^3}{U_w \nu}$$

is the local Rayleigh number.

4. Numerical Approach by using CCM

The MHD chemically reactive of Casson non-Newtonian nanofluid flow equations, the Chebyshev collocation scheme was used to make an approximation solution. The basic functions used in the process of solving the governing ODEs are described as a Chebyshev polynomial. The following components make up this technique: Assuming that the coefficients of the functions that depend on the Chebyshev collocation scheme solutions in the differential equations are unknown, the predicted results are substituted into the expressions that govern the scheme in order to generate residuals or errors. The assumed results are substituted into the expressions that control the scheme in order to generate residual errors. Subsequently, the scheme of collocation is utilized in order to minimize the residual errors. An algebraic expression must be generated and then computed in order to find the unknown coefficient values. The accuracy of the expression was improved by making a mapping for shifted Chebyshev from [0, 1] to [0, ∞] [35 and 36]. CCM is used here to numerically solve the boundary value problem in (8) - (11) , where the following assumptions are made about the solutions for unknown functions $f(\eta), \theta(\eta)$ and $\phi(\eta)$ for the sum of the Chebyshev base function:

$$f(\eta) = \sum_{i=0}^{N} a_i T_i\left(\frac{2\eta}{L} - 1\right),\quad \theta(\eta) = \sum_{i=0}^{N} b_i T_i\left(\frac{2\eta}{L} - 1\right)$$
$$\text{and } \phi(\eta) = \sum_{i=0}^{N} c_i T_i\left(\frac{2\eta}{L} - 1\right) \quad (15)$$

To calculate the values of undetermined coefficients, equation (15) is substituted into (8) - (10) and becomes then

$$\left(1 + \frac{1}{\beta}\right)\left[(1 + \in_2 - \in_2 \theta) F_{\eta\cdot 3} - \in_2 \theta_\eta F_{\eta\cdot 2}\right] - F_\eta^{\ 2}$$
$$+ FF_{\eta\cdot 2} - \frac{M}{(1+\varepsilon\theta)} F_\eta + G_r\theta + G_c\phi - \quad (16)$$
$$P_p\left(1 + \frac{1}{\beta}\right)(1 + \in_2 - \in_2 \theta) F_\eta - F_s F_\eta^{\ 2} = 0$$

For $j = 1, 2, \Lambda, N-1$

$$\theta_{\eta\cdot 2}+\in_4\theta\theta_{\eta\cdot 2}+\in_4\theta_\eta^{\,2}+P_rF\theta_\eta+$$
$$P_rN_b\theta_\eta\phi_\eta+P_rN_t\theta_\eta^{\,2}+\delta\theta+\frac{P_rME_c}{(1+\varepsilon\theta)}F_\eta^{\,2}$$
$$+P_rE_c\left(1+\frac{1}{\beta}\right)(1+\in_2-\in_2\theta)F_{\eta\cdot 2}^{\,2}+ \quad (17)$$
$$\frac{4}{3}N\theta''+P_rP_pE_c\left(1+\frac{1}{\beta}\right)(1+\in_2-\in_2\theta)F_\eta^{\,2}$$
$$+P_rE_cF_sF_\eta^{\,3}+AF_\eta+A^*\theta=0$$

For $j=1,2,\Lambda\ ,N-1$

$$\phi_{\eta\cdot 2}+\in_6\theta\phi_{\eta\cdot 2}+\in_6\theta_\eta\phi_\eta+LeF\phi_\eta+$$
$$\frac{N_t}{N_b}\theta_{\eta\cdot 2}-Le\lambda(1+\delta_w\theta)^m e^{-\frac{E}{(1+\delta_w\theta)}}\phi=0 \quad (18)$$

For $j=1,2,\Lambda\ ,N-1$While the boundary conditions becomes.

$$\begin{cases} F(0)=S,\ F_\eta(0)=\xi+\left(1+\frac{1}{\beta}\right) \\ ,\theta(0)=1,\ \phi(0)=1, \\ F_\eta(\infty)\to 0,\ \ \theta(\infty)\to 0,\ \phi(\infty)\to 0 \end{cases} \quad (19)$$

Residues $R_f(\eta, a_i, b_i)$, $R_\theta(\eta, a_i, b_i, c_i)$ and $R_\phi(\eta, a_i, b_i, c_i)$are obtained by plugging into equation (16), (17), (18) and (19). Using the collocation approach, the residues are reduced to the smallest

$$\text{For } \delta(\eta-\eta_k)=\begin{cases}1, & \eta=\eta_k \\ 0, & otherwise\end{cases} \quad (20)$$

$$\int_0^L R_f\delta(\eta-\eta_k)d\eta=R_f(\eta_j)=0,$$
$$for\ j=1,2,\Lambda\ ,N-1$$
$$\int_0^L R_\theta\delta(\eta-\eta_k)d\eta=R_\theta(\eta_j)=0, \quad (21)$$
$$for\ j=1,2,\Lambda\ ,N-1$$
$$\int_0^L R_\phi\delta(\eta-\eta_k)d\eta=R_\phi(\eta_j)=0,$$
$$for\ j=1,2,\Lambda\ ,N-1$$

Where $\eta_j=\frac{L}{2}\left(1-\cos\left(\frac{j\pi}{N}\right)\right)$ is the shifted Gauss-Lobatto point.

In this manner, equations (16) to (21) form a system of $3N+3$ algebraic equations with $3N+3$ unknown constant coefficients, a_i, b_i and c_i. The resulting algebraic equations were solved, and the values of constant coefficients are found using the MATHEMATICA version 11.3 program. The value of L is set to 12 to ensure that all numerical solutions accurately respect the far-field asymptotic.

5. Results and Discussion

To get a clear understanding of the magnetohydrodynamic (MHD) chemically reactive of Casson non-Newtonian nanofluid flow. In this section, the numerical solutions of velocity, heat propagation, and plate wall heat gradient are presented. Figure. 2 indicate that increasing the thermal Grashof number increases the speed of the fluid flow. The flow is accelerated by an increase in buoyant force, which corresponds to an increase in the thermal Grashof number. Positive thermal Grashof numbers correspond to natural convection cooling of the plate. As a result, heat is transported from the vertical plate to the fluid, increasing the temperature and buoyancy force. Furthermore, when the thermal Grashof number increases, the velocity nears the plate and then gently decays to the free stream velocity. The influence of various mass Grashof numeric values on the velocity field is seen in Figure 3. The proportion of the concentration buoyancy effect to the viscous hydrodynamic pressure is defined as the mass Grashof number. As the mass Grashof number grows, the velocity seems to increase. The impact of porosity on velocity profile is shown in Figure. 4, which reveal an increase in porosity as a result of an increase in fluid viscosity, a drop in fluid flow velocity due to a decrease in the accelerating surface's stretching rate or a fall in permeability near the edge. Because of this, the velocity distribution is altered. Figure 5 depicts the combined influence of the chemical reaction parameter and the variable viscosity parameter. An

increase in the temperature differential $(T_w - T_\infty)$, which reduces the fluid's dynamic viscosity, may raise the fluid's velocity by increasing the variable viscosity parameter and the chemical reaction parameter, respectively. As a result, the fluids velocity rises. The yield stress is seen in Figure 6 to be suppressed when the Casson parameter is increased. Lorentz force is a drag force that acts to slow down fluid flow, hence raising the magnetic field parameter reduces flow velocity because it induces a Lorentz force that acts to slow down fluid flow. As a consequence, the combined effect of the Casson and magnetic field parameters causes the velocity profile to drop. The effect of the Casson parameter and electric conductivity on a temperature profile is seen in Figure. 7. Increases in the Casson parameter lower flow but encourage temperature rise; also, increases in the fluid's electric conductivity tend to raise the temperature profile of the flow. Figure 8 examines the influence of *Ec* and $(\in_4)$ on the temperature distribution. The temperature profile is seen to reduce as the variable thermal conductivity values rise. As a result, the temperature profile is reduced as the fluid's $\in_4$ rises, resulting in faster heat transfer from the fluid to the wall and thereby lowering the temperature. In Figure. 9, the effect of Ra and the *Pr* on the temperature distribution is examined. The figure indicates that the growth in thermo-physical properties tends to decrease the temperature distributions. The Prandtl number has an impact on the relative thickness of the movement and thermal boundary layers. Since the Prandtl number has a low thermal conductivity, it serves to decrease boundary layer thickness; also, as the thermal radiation parameter increases, less heat is carried, and less radiative heat is conveyed due to a significant reduction in temperature distribution. The effect of variable mass diffusion and magnetic parameters on the concentration profile is depicted in Figure. 10. The graph demonstrates that when both parameters grow, so does the concentration profile. Increased variable mass diffusion improves the concentration profile. Similarly, when the magnetic parameter increases, the effect of velocity fluctuation has a major influence on the concentration profile. The effect of Nt and the Nb on the concentration profile is seen in Figure 11. The influence of Brownian motion and the thermophoresis on the concentration profile is seen in Figure 11. Increased Brownian motion causes heat diffusion from the surface to the boundary layer, which favors concentration increase. However, increasing the value of the thermophoresis parameter result in stronger thermophoretic force, which draws particles from the fluid to the wall surface, raising the temperature and hence lowering the concentration profile. The comparison results of the Nusselt number of some existing literature: Khan and Pop [26], Makinde and Aziz [27], under some certain conditions ($\varepsilon = \varepsilon_2 = \varepsilon_4 = S = M = P_P = F_S = A = A^* = 0, \beta \to \infty$ and absence of nanoparticles) were tabulated on Table.1. Table.2 illustrated the behaviour of Nusselt number and Sherwood number for different parameters.

Table 1
Comparison table for values of P_r

P_r	$(-\theta'(0))$ Present Study	$(-\theta'(0))$ [26]	$(-\theta'(0))$ [27]
0.2	0.1734	0.1691	0.1691
0.7	0.4539	0.4539	0.4539
2.0	0.9114	0.9114	0.9114

Table 2
Nusselt number $(Ra_x^{-0.25} Nu)$ and Sherwood number $(Ra_x^{-0.25} Sh)$ for different parameter values.

N_t	N_b	A	A^*	$(Ra_x^{-0.25} Nu)$	$(Ra_x^{-0.25} Sh)$
1.0				2.401162	1.288832
1.5				2.552038	1.325120
2.0				2.558877	1.658279
	1.0			1.643716	4.863222
	1.5			1.547902	3.287746
	2.0			1.328745	2.372643
		0.1		2.046715	1.348907
		0.2		2.115544	1.371841
		0.5		2.182293	1.3940962
			1.5	2.646401	1.548805
			2.5	2.733752	1.5779164
			3.0	2.814041	1.604682

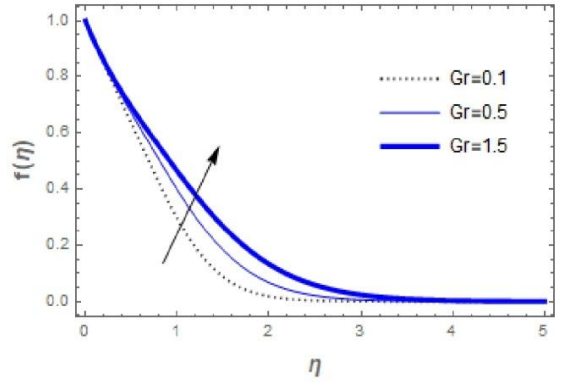

Fig. 2: Influence of G_r on fluid flow

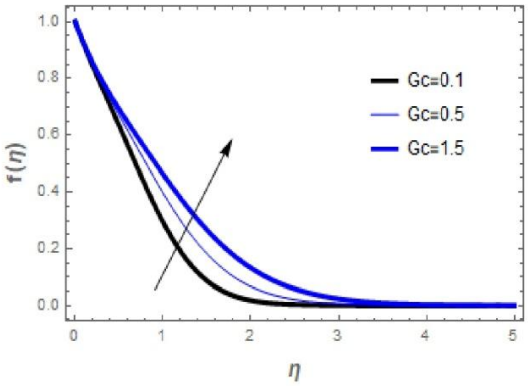

Fig. 3: Influence of G_c on velocity profile

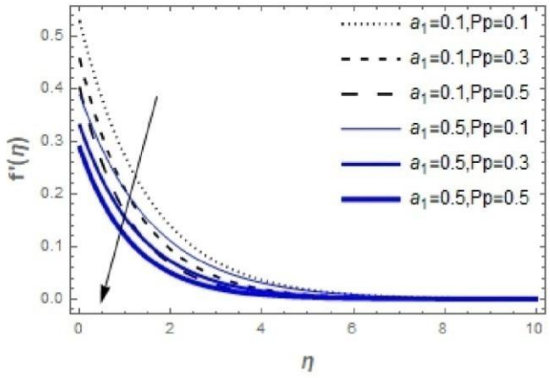

Fig. 4: Influence of a_1 and P_p on fluid flow

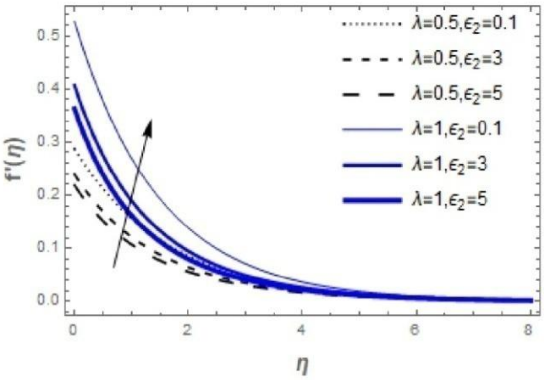

Fig. 5: Effect of λ and $\in_2$ on fluid flow

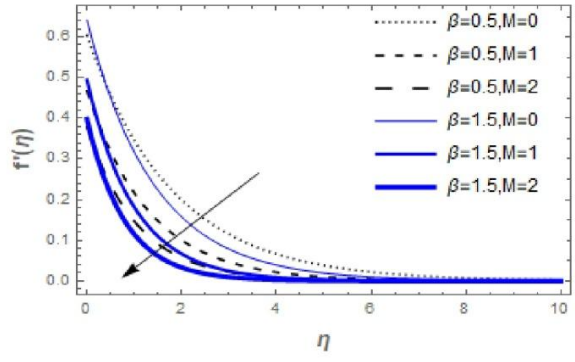

Fig. 6: Influence of β and M on fluid flow

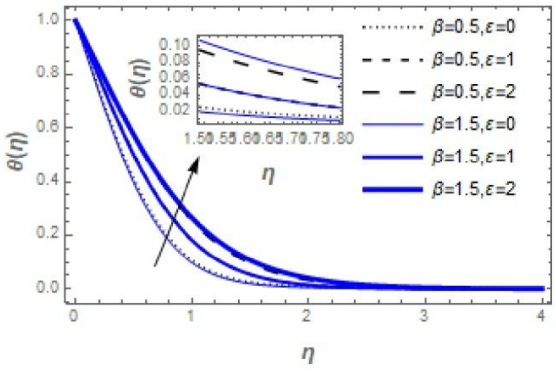

Fig. 7: Influence of β and ε on thermal field

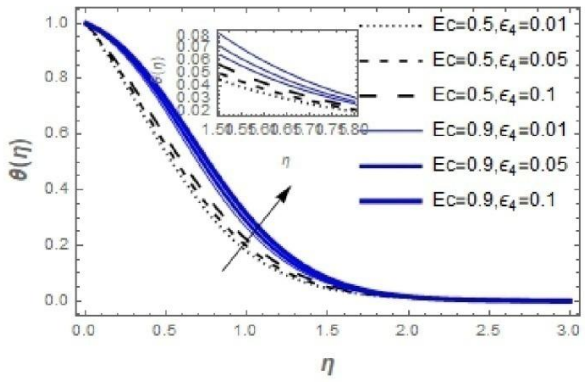

Fig. 8: Influence of E_c and $\in_4$ on thermal field field

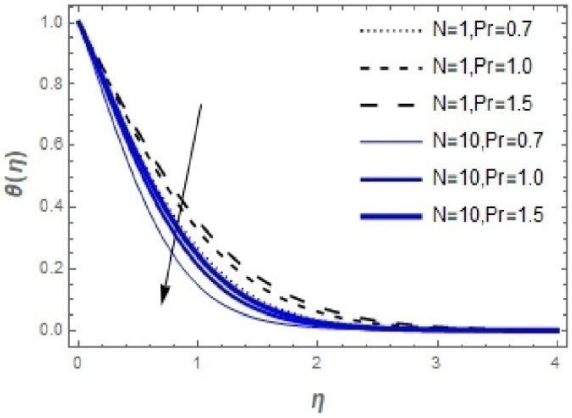

Fig. 9: Influence of N and P_r on thermal

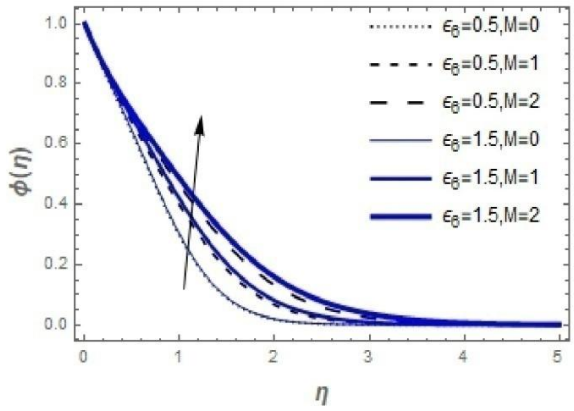

Fig. 10: Influence of $\in_6$ and M on on concentration profile

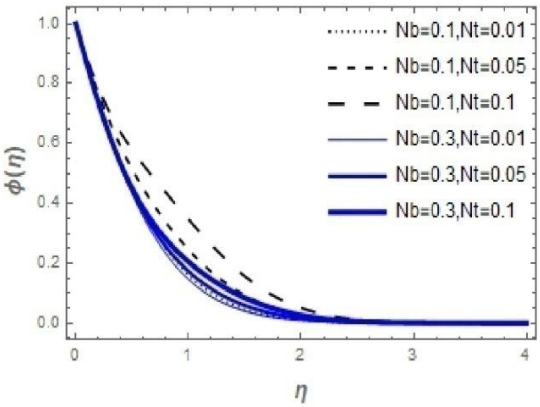

Fig. 11: Influence of N_b and N_t concentration profile

5. Conclusions

In this article, the numerical investigation of the MHD chemically reactive Casson non-Newtonian nanofluid flow on a two-dimensional incompressible steady from a stretched sheet in a porous quiescent medium with buoyancy effect is presented. The current CCM demonstrates a high numerical efficiency in producing quick, accurate results with a low simulation effort and less iteration performance. The PDEs were converted with the help of a similarity variable, and the resulting non-linear ODEs were solved using CCM with the help of the MATHEMATICA 11.3 program. The influence of the following factors on the velocity, temperature, and concentration profiles is taken into account. The following are the resulting conclusions.

(1) The temperature profile rises as the Casson parameter and electric conductivity rise.

(2) Velocity profiles are increased when the thermal and mass Grashof number are increased. Consequently, both parameters contribute to the buoyancy effect of the fluid.

(3) The velocity profile is reduced when the Porosity, Casson, and magnetic parameters are reduced.

(4) The temperature profile is increased with a greater Eckert number, but it decreases with an increase in the variable thermal conductivity parameter.

(5) The temperature profile drops as thermal radiation and the Prandtl number increase.

(6) Increase the concentration profile by increasing the magnetic parameter and the variable mass diffusion parameter.

(7) Grater Brownian motion parameter

values promote the concentration profile, while larger Thermophoresis parameter values depreciate it.

Acknowledgment

The authors acknowledge the Department of Pure and Applied Mathematics, Ladoke Akintola University of Technology's superb research facilities.

Data Availability Statement

This research paper contains all of the data and materials created during this investigation. There is data linked with this paper in a data repository. [Author's comment: All data used in this work may be acquired from the respective author upon request.]

Conflict of Interests

There are no competing interests declared by the author(s).

References

[1] R. G. Becker, W. C. Morgan, J. E. Chin, J. Griffith. Improved Rheology Model and Hydraulics Analysis for Tomorrow's Wellbore Fluids Application; Society of Petroleum Engineers, Tulsa, Oklahoma. (2003) https://doi.org/10.2118/82415-MS

[2] J. F. Steffe. Rheological Methods in Food Processing Engineering (6^{th}ed.) Freeman press. East Lansing USA.(1996)ISBN 0-9632036-1-4.

[3] F. J. Adewale, A. P. Lucky, A. P. Oluwabunmi, E. F. Boluwaji. Selecting the Most Appropriate Model for Rheological Characterization of Synthetic Based Drilling Mud; International Journal of Applied Engineering Research. (2017). 12(18) 7614-7629. ISSN 0973-4562.

[4] M. Ramzan, N. Shaheen, J. D. Chung, S. Kadry, Y. M. Chu, F. Howari. Impact of Newtonian heating and Fourier and Fick's laws on a MHD dusty Cassonnanofluid flow with variable heat source/sink over a stretching cylinder; Scientific Reports 11, article number: 2357 (2021). http://dx.doi.org/10.1038/s41598-021-81747-x.

[5] G. Murali, P. Ajit, N. V. N. Babu. Numerical study of chemical reaction on unsteady MHD fluid flow past an infinite vertical plate embedded in a porous medium with variable suction. Electronic Journal of Mathematical Analysis and Applications, (2015)Vol. 3(2). Pp. 179-192. http://fcagegypt.com/Journal/EJMAA/

[6] S. D. Yahaya, K. D. Simon. Effects of buoyancy and thermal radiation on MHD flow over a stretching porous sheet using homotopy analysis method; Alexandria Engineering Journal. (2015).54, 705–712.

[7] A. O. Akindele, O. A. Ajala, P. Adegbite, A. W. Ogunsola. Convective Flow of Nanofluids Using Blasius-Rayleigh-Stoke Variable with Slip Effect, IOSR Journal of Mathematics (2021). (IOSR-JM) e-ISSN: 2278-5728. 17(3) 01-08, p-ISSN: 2319-765X

[8] A. S. Oke, W. N. Mutuku, M. Kimathi, I. L. Animasaun. Insight into the dynamics of non-Newtonian Casson fluid over a rotating non-uniform surface subject to Coriolis force.Nonlinear Engineering; (2020). 9: 398–411, https://doi.org/10.1515/nleng-2020-0025

[9] A. J. Chamkha. Thermal radiation and buoyancy effects on hydromagnetic flow over an accelerating permeable surface with heat source or sink.Int. J. Eng. Sci. (2000) 38 (15) 1699–1712.

[10] M. Gilbert, S. Shaw, P. Sibanda. Diffusion of chemically reactive species in Casson fluid flow over an Unsteady Stretching surface in porous medium in the presence of a magnetic field; Mathematical Problems in Engineering, Volume (2015), Article ID 724596, 10 pages, http://dx.doi.org/10.1155/2015/724596

[11] S. Pramanik. Casson fluid flow and heat transfer past an exponentially porous stretching surface in presence of thermal radiation. Ain Shams Engineering Journal (2014). 5, 205–212.

[12] M. Meraj, T. Hayat, I. Pop, A. Hendi. Stagnation-Point Flow and Heat Transfer of a Casson Fluid towards a Stretching Sheet; ZeitschriftNaturforsch. (2012). 67a, 70 – 76. DOI: 10.5560/ZNA.2011-0057.

[13] N. S. Kumar. Analytical Solution of MHD Stagnation-Point Flow and Heat Transfer of Casson Fluid over a Stretching Sheet with Partial Slip; ISRN ThermodynamicsVol. (2013), Article ID 108264, 9 pageshttp://dx.doi.org/10.1155/2013/108264

[14] D. S. Sankar, B. Maziri, H. Morsidi. Mathematical Analysis Of Casson Fluid Flow Through Elastic Tube With Applications To Blood Flow; Advances and Applications in Fluid Mechanics, (2016)19(3) 489-506, ISSN: 0973-4686, http://dx.doi.org/10.17654/FM019030489.

[15] A. M. Obalalu, O. A. Ajala, A. Abdulraheem, A. O. Akindele. The influenceof variable electrical conductivity on non-

DarcianCassonnanofluid flow with first and second-order slip conditions. Partial Differential Equations in Applied Mathematics. (2021). 4, 100084.

[16] A. M. Obalalu, O. A. Ajala, A. A. Taofeeq. Natural Convective Non-Newtonian Casson Fluid Flow in a Porous Medium with Slip and Temperature Jump Boundary Conditions; PetrolCoal.(2020)62(4): 1532-1545 ISSN 1337-7027 https://www.researchgate.net/publication/348232894

[17] A. E. Maurice, I. Y. Seini, L. B. Bortteir. Analysis of Casson Fluid Flow over a Vertical Porous Surface with Chemical Reaction in the Presence of Magnetic Field; Journal of Applied Mathematics and Physics. (2015). 3, 713-723 http://dx.doi.org/10.4236/jamp.2015.36085.

[18] D. Khan, A. Khan, I. Khan, F. Ali, F. Karim, I. Tlili. Effects of Relative Magnetic Field, Chemical Reaction, Heat Generation and Newtonian Heating on Convection Flow of Casson Fluid over a Moving Vertical Plate Embedded in a Porous Medium; Scientific reports.(2019). 9:400. DOI: 10.1038/s41598-018-36243-0.

[19] A. A. Taofeeq, J. A. Gbadeyan, R. S. Lebelo. Heat Transport of CassonNanofluid Flow over a Melting Riga Plate Embedded in a Porous Medium; International Journal of Engineering Research in Africa (2021). ISSN: 1663-4144, 55- 15-27 doi:10.4028/www.scientific.net/JERA.55.15

[20] A. O. Akindele, A. W. Ogunsola. A study of non-isothermal permeable flow of nano-fluid in a stretchable rotating disk system. J. Math. Comput. Sci. (2021) 11, No. 2, 1486-1498. ISSN: 1927-5307.

[21] A. W. Ogunsola, A. O. Akindele. Mixture of Al_2O_3-Cu/H_2O-$(CH_2OH)_2$ MHD hybrid nanofluid flow due to a stretchable rotating disks system under the influence of non-uniform heat source or sink and thermal radiation. J. Math. Comput. Sci, (2022), 12:8. ISSN: 1927-5307.https://doi.org/10.28919/jmcs/6624.

[22] A. M. Obalalu, A. O. Ajala, A. O. Akindele, O. A. Oladapo, A. O. Adepoju, O. M. Jimoh. Unsteady squeezed flow and heat transfer of dissipative casson fluid using optimalhomotopy analysis method: An application of solar radiation. Partial Diff Equ ApplMath. (2021):100146. http://dx.doi.org/10.1016/j.padiff.2021.100146.

[23] A. O. Akindele, A. W. Ogunsola, A. M. Obalalu, P. Adegbite, O. A. Ajala, S. Alao. Mhd flow of nano-fluid with non-uniform heat source or sink in the presence of chemical reaction and activation energy. Journal of Advance Research in Applied Science(2021) ISSN: 2208-2352.Volume-8 | Issue-5.

[24] A. M. Obalalu, O. A. Ajala, A. O Akindele, S. Alao, O. A. Adepoju. Effect of melting heat transferon electromagnetohydrodynamic non-newtoniannanofluid flow over a riga plate with chemical reactionand arrhenius activation energy; Eur. Phys. J. Plus (2021) 136:891.https://doi.org/10.1140/epjp/s13360-021-01869-z.

[25] A. M. Obalalu, O. A. Ajala, T. A. Adeosun, A. O. Akindele, O. A. Oladapo, O. A. Olajide, P. Adegbite. Significance of variable electrical conductivity on non-Newtonian fluid flow between two vertical plates in the coexistence of Arrhenius energy and exothermic chemical reaction.Partial Diff Equ ApplMath. (2021):https://doi.org/10.1016/j.padiff.2021.100184.

[26] W. Khan, I. Pop. Boundary-layer flow of a nanofluid past a stretching sheet. Int JHeat. (2010);53 (11–12): 2477–2483.http://dx.doi.org/10.1016/j.ijheatmasstransfer.2010.01.032.

[27] O. D. Makinde, A. Aziz. Boundary layer flow of a nanofluid past a stretching sheet with a convective boundary condition. Int J Therm Sci. (2011); 50(7): 1326–1332.http://dx.doi.org/10.1016/j.ijthermalsci.2011.02.019.

[28] L. Ali, B. Ali, M. B. Ghori. Melting effect on Cattaneo–Christov and thermal radiation features for aligned MHD nanofluid flow comprising microorganisms to leading edge: FEM approach. Computers & Mathematics with Applications. 2022 Mar 1; 109: 260-9.

[29] L. Ali, B. Ali, X. Liu, S. Ahmed, M. A. Shah. Analysis of bio-convective MHD Blasius and Sakiadis flow with Cattaneo-Christov heat flux model and chemical reaction. Chinese Journal of Physics. 2022 Jun 1; 77: 1963-75.

[30] L. Ali, B. Ali, X. Liu, T. Iqbal, R. M. Zulqarnain, M. Javid. A comparative study of unsteady MHD Falkner–Skan wedge flow for non-Newtonian nanofluids considering thermal radiation and activation energy. Chinese Journal of Physics. 2022 Jun 1; 77: 1625-38.

[31] L. Ali, B. Ali, A. M. Allah, Z. Hammouch, S. Hussain, I. Siddique, Y. Huang. Insight into significance of thermal stratification and radiation on dynamics of micropolar water based TiO2 nanoparticle via finite element simulation. Journal of Materials Research and Technology. 2022 Jul 1;19: 4209-19.

[32] L. Ali, Y. J. Wu, B. Ali, S. Abdal, S. Hussain. The crucial features of aggregation in TiO2-water nanofluid aligned of chemically comprising microorganisms: A FEM approach. Computers & Mathematics with Applications. 2022 Oct 1;123:241-51.

[33] L. Ali, B. Ali, D. Habib, Q. A. Mdallal. Finite element analysis on the thermo-convective non-isothermal nanofluid flow in MHD Hall generator system with Soret and Dufour effects. Case Studies in Thermal Engineering. 2022 Nov 1;39:102389.

[34] A. M. Obalalu, A. O. Ajala, A. O. Akindele, O. A. Oladapo, O. A. Olajide, O. M. Jimoh. Computational study of magneto-convective non-Newtonian nanofluid slip flow over a stretching/shrinking sheet embedded in a porous medium. Computers & Mathematics with Applications. Volume 119, 1 August 2022, Pages 319-326.

[35] S. O. Salawu, A. M. Obalalu, E. O. Fatunmbi, R. A. Oderinu. Thermal Prandtl-Eyring hybridized MoS2-SiO2/C3H8O2 and SiO2-C3H8O2 nanofluids for effective solar energy absorber and entropy optimization: A solar water pump implementation. Journal of Molecular Liquids, (2022)1, 119608.

[36] S. O. Salawu, A. M. Obalalu, S. S. Okoya. Thermal convection and solar radiation of electromagnetic actuator Cu–Al2O3/C3H8O2 and Cu–C3H8O2 hybrid nanofluids for solar collector optimization. Materials Today Communications, 33, 104763.

[37] B. S. Goud. Thermal radiation influences on MHD stagnation point stream over a stretching sheet with slip boundary conditions. International Journal of Thermofluid Science and Technology. 2020; 7(2).

[38] A. K. Patra, M. K. Nayak, A. Misra. Viscosity of nanofluids-A Review. International Journal of Thermofluid Science and Technology. 2020; 7(2): 070202.

[39] Y. H. Gangadharaiah, S. P. Suma, H. Nagarathnamma, T. Y. Chaya. Double-diffusive penetrative convection in a fluid overlying a porous layer." International Journal of Thermofluid Science and Technology. (2021)